Monte Carlo study of the two–dimensional site–diluted dipolar Ising model

Juan J. Alonso[1,*] and B. Allés[2,†]

[1] *Física Aplicada I, Universidad de Málaga, 29071 Málaga, Spain*
[2] *INFN–Sezione di Pisa, Largo Pontecorvo 3, 56127 Pisa, Italy*

(Dated: April 5, 2010)

By tempered Monte Carlo simulations, we study 2D site–diluted dipolar Ising systems. Dipoles are randomly placed on a fraction x of all L^2 sites in a square lattice, and point along a common crystalline axis. For $x_c < x \leq 1$, where $x_c = 0.79(5)$, we find an antiferromagnetic phase below a temperature which vanishes as $x \to x_c$ from above. At lower values of x, we study *(i)* distributions of the spin–glass (SG) overlap q, *(ii)* their relative mean square deviation Δ_q^2 and kurtosis and *(iii)* ξ_L/L, where ξ_L is a SG correlation length. From their variation with temperature and system size, we find that the paramagnetic phase covers the entire $T > 0$ range. Our results enable us to obtain an estimate of the critical exponent associated to the correlation length at $T = 0$, $1/\nu = 0.35(10)$.

PACS numbers: 75.10.Nr, 75.10.Hk, 75.40.Cx, 75.50.Lk
Keywords:

I. INTRODUCTION

In the last years, there has been a renewed interest in systems of interacting dipoles (SIDs). This is in part due to recent advances in nanoscience[1] which make realizations of assemblies of magnetic nanoparticles available.[2,3] Empirically, these systems show a rich collective behavior in which the dipole–dipole interaction plays a key role that can be observed at low (but experimentally accessible) temperatures. Dipoles forming crystalline arrays exhibit long–range ferro or antiferromagnetic order that depends crucially on lattice geometry[4,5] because of geometric frustration caused by the spatial variations of the directions of dipolar fields. Two–dimensional (2D) arrays of cobalt–ferrite and Co nanoparticles placed on hexagonal arrays have been found to exhibit in–plane short–range ferromagnetic order.[6] On the contrary, arrays on a square lattice composed of Mn As ferromagnetic nanodisks epitaxially grown on a substrate exhibit collinear AF patterns.[7]

Magnetic ordering of SIDs depends also on anisotropy. On the one hand, dipolar–dipolar interactions create effective anisotropies that in square lattices, for example, push spins to lie on the plane of the lattice.[8] On the other hand, magnetocrystalline site–anisotropy energies of the crystallites that form the nanoparticles are often greater than dipolar–dipolar interparticle energies. This is the case of the arrays of Mn As ferromagnetic nanodisks we mention above, that behave as a system of Ising dipoles with their magnetic moment rigidly aligned along the in–plane crystalline easy axes of the nanodisks.[7] In such a case, the resulting magnetic order depends on the competition of dipolar and anisotropic energies. Crystalline Ising dipolar systems (IDSs) are reasonable models for these planar systems.[9] Some ferroelectrics,[10] insulating magnetic salts as $LiHoF_4$, as well as some three–dimensional (3D) crystals of organometallic molecules[11] are known to be well described by arrays of IDSs.[9,12]

SIDs in disordered spatial arrangements are particularly interesting. The presence of spatial disorder, together with the geometric frustration generated by dipolar interactions, gives rise to random frustration that may result in SG behavior. In fact, some non–equilibrium SG behavior (like time dependent susceptibilities and memory effects) has been observed in experiments with systems of randomly placed nanoparticles or very diluted magnetic crystals.[10,13] Furthermore, Monte Carlo (MC) simulations have given clear evidence of the existence of a transition at finite temperature T_{SG} from a paramagnetic to an equilibrium SG phase in systems of randomly oriented axis dipoles (RADs) placed either on fully occupied or on diluted simple cubic (SC) 3D lattices, and $T_{SG} = 0$ instead for 2D square lattices.[14] Recent numerical work has reported a SG transition in a model of parallel axis dipoles (PADs) placed on a lattice that approximates that of the diluted[15] $LiHo_xY_{1-x}F_4$, a material for which such a transition has been reported,[16] (albeit not without some controversy[17]). By MC simulation the whole phase diagram of site–diluted PADs placed on a 3D SC lattice has been obtained[18] as a function of the concentration x. It includes a SG phase for $0 < x \lesssim 0.65$ which, strikingly, has been found to behave marginally, that is, it has quasi–long range order, as in the 2D XY model.[19] This is contrary to theoretical expectations,[20,21] that SG systems with long–range interactions may behave as short–range Edwards–Anderson (EA) models,[22] which in 3D are believed to have a SG phase with a non–vanishing order parameter (according to the RSB[23] or droplet[24] pictures of SGs).

Then, in order to get a deeper understanding of SG systems beyond the already extensively studied random–bond models with short–range interactions, it makes sense to analyze the behavior of the 2D PAD model and compare it with the short–range 2D EA model. The latter had been found to have an algebraic divergence at $T_{SG} = 0$ with critical exponent[25] $1/\nu = 0.50(5)$, although more recent simulations for larger systems and lower temperatures give a value of $1/\nu = 0.29(4)$ for Gaussian interactions.[26]

Our purpose is the study by MC simulations the phase

diagram of a site–diluted system of magnetic dipoles. They are placed at random on the sites of a square lattice and point up or down along a given principal axis. Since in the limit of low concentrations every detail of the lattice is expected to become irrelevant,[18] our results have direct connection with some of the work we describe above. Our intention is to search for the temperature T_{SG} of a possible SG transition and study the related divergence of the correlation length. Further, we aim to study whether the diluted PAD model belongs to the same universality class recently conjectured,[27] though not reliably shown by MC simulations,[28] for the set of 2D EA Ising models with varying quenched disorder.

The plan of the paper is as follows. In Section II we define the model and give details on the parallel tempered Monte Carlo (TMC) algorithm[29] used for updating. We also define the quantities we calculate. They include the spin overlap[30] q and a correlation length[22,31] ξ_L. In Section III A we give results for the dipolar AF phase for $x > x_c$, where $x_c = 0.79(5)$, as well as for its nature and boundary. In Section III B, numerical results are shown for distributions of q and ξ_L/L at $x = 0.2$ and 0.5. We examine the evidence against the existence of a finite temperature SG phase transition when $x < x_c$: *(i)* the mean values $\langle \mid q \mid \rangle$ and $\langle q^2 \rangle$ decrease faster than algebraically with L as L increases for $T/x \gtrsim 0.3$, *(ii)* double peaked, but wide, distributions of $q/\langle \mid q \mid \rangle$ change with L for temperatures as low as $T/x = 0.4$, and *(iii)* kurtosis and ξ_L/L decrease with L at all T and do not cross, as it would be expected for a finite temperature transition. Scaling plots for g and ξ_L/L are given in Section III C. Our results are consistent with a ratio ξ_L/L that diverges with exponent $1/\nu = 0.35(10)$. Results are summarized in Section IV.

II. MODEL, METHOD, AND MEASURED QUANTITIES

A. Model

We treat site–diluted systems of Ising magnetic dipoles (also named spins in this paper) on a 2D square lattice. At each lattice site a dipole is placed with probability x. Then, the number N of spins on the lattice is less than L^2 (L is the lateral size of the lattice) approximately by a factor x. Site i is said *occupied* if it contains one spin. All dipoles are parallel and point along the Y axis of the lattice. This axis shall be called *spin axis*. The Hamiltonian is given by,

$$H = \frac{1}{2} \sum_{i \neq j} T_{ij} \sigma_i \sigma_j \,, \tag{1}$$

where the sum runs over all occupied sites i and j except $i = j$, $\sigma_i = \pm 1$ on any occupied site i and

$$T_{ij} = \varepsilon_a (a/r_{ij})^3 (1 - 3y_{ij}^2/r_{ij}^2). \tag{2}$$

If $\mathbf{r}_{ij}$ is the vector joining sites i and j, then $r_{ij} = \|\mathbf{r}_{ij}\|$ is its modulus and y_{ij} its Y component. ε_a is an energy and a is the lattice spacing. In the following all temperatures and energies shall be given respectively in units of ε_a/k_B (k_B is the Boltzmann constant) and ε_a.

Due to the long–range nature of the dipolar interactions, we are able to simulate on rather small lattice sizes ($L \leq 32$).

Strength T_{ij} is the usual long–range dipole–dipole interaction. Note that T_{ij} signs are not distributed at random, but depend on the orientation of $\mathbf{r}_{ij}$ vectors on the lattice. Randomness in our model arises only through the introduction of the probability x for placing dipoles. This is to be contrasted with random–bond EA Ising models with bond strengths $J_{ij} = \varepsilon_{ij}/r_{ij}^{\mu}$ where ε_{ij} are chosen at random from a bimodal or Gaussian distribution with zero mean[21] and μ is a real exponent. This is why PADs exhibit AF order at high concentration in contrast to these models that do not. Similar statements apply when our PAD model is compared with a random–axes dipolar model (RAD), in which Ising dipoles lie along directions chosen at random for each site.[14]

B. Method

Periodic boundary conditions (PBC) are imposed. Spins on occupied sites i have been allowed to interact only with spins j within an $L \times L$ squared box centered on site i. This method unambiguously defines the vector $\mathbf{r}_{ij}$ to be used in (2) and also excludes interactions with spins belonging to the repeated copies of the lattice that appear beyond the boundary. Because of the long–range nature of dipolar interactions, contributions from beyond this box would have been taken into account (for example by means of Ewald's summations[32]) if spins were to form ferromagnetic domains. They do not do so in our PAD model. In all simulations presented in this work we have found $T\chi_F \lesssim 1$, where χ_F is the ferromagnetic susceptibility. Therefore those contributions do not affect the thermodynamic limit regardless of the kind of phase the system lies (paramagnetic, AF or SG). Some details on this point are found in.[18]

In order to circumvent large energy barriers that could slow down the evolution of the system, in particular from certain states representing minima of the energy (mainly at low temperatures), we have used the TMC algorithm.[29] It consists in running in parallel a set of n identical systems at equally spaced temperatures T_i, given by $T_i = T_1 - (i-1)\Delta T$ ($i = 1, \cdots, n$ and $\Delta T > 0$) where each system i is cyclically allowed to exchange its state with system $i+1$. Each system evolves independently by use of the standard single–spin–flip Metropolis algorithm[33] and whenever a single flip is accepted, all dipolar fields throughout the entire lattice are updated.

In detail the procedure is as follows:[14,18] *(1)* a cycle on i is run from $i = 1$ to $i = n$; *(2)* when the cycle arrives at system i, 8 Metropolis steps are applied on it; *(3)* next,

TABLE I: Simulation parameters. x is the probability for sites to be occupied with a magnetic dipole; L is the lateral lattice size; ΔT is the temperature step in the TMC runs; T_1 and T_n are the highest and lowest temperatures, respectively; N_r is the number of pairs of quenched disordered samples; t_0 is the number of MC sweeps. The measuring time interval is $[t_0, 2t_0]$ in all cases.

$x = 0.2$, $\Delta T = 0.02$, $T_1 = 0.6$, $t_0 = 4 \times 10^7$						
L	8	12	16	20	24	32
T_n	0.04	0.04	0.04	0.04	0.04	0.08
N_r	2400	550	1500	650	700	200
$x = 0.5$, $\Delta T = 0.05$, $T_1 = 2$, $T_n = 0.1$, $t_0 = 8 \times 10^6$						
L	8	16	20	24		
N_r	2500	2500	350	250		
$x = 0.6$, $T_n = 0.2$, $t_0 = 4 \times 10^6$						
L	8	16	20	24		
T_1	3	3	2	2		
ΔT	0.2	0.2	0.1	0.1		
N_r	1200	300	300	300		
$x = 0.7$, $\Delta T = 0.1$, $T_1 = 2$, $T_n = 0.2$						
L	8	16	20	24		
t_0	8×10^5	8×10^5	4×10^6	4×10^6		
N_r	4200	2200	400	100		
$x = 0.8$, $\Delta T = 0.1$, $T_1 = 3$, $T_n = 0.2$						
L	8	16	20	24		
t_0	8×10^5	8×10^5	4×10^6	4×10^6		
N_r	4500	1200	500	350		
$x = 0.86$, $\Delta T = 0.1$, $T_1 = 3$, $T_n = 0.2$, $t_0 = 8 \times 10^5$						
L	8	16	20	24		
N_r	3000	400	300	70		
$x = 0.9$, $\Delta T = 0.1$, $T_1 = 3$, $T_n = 0.2$, $t_0 = 8 \times 10^5$						
L	8	16	20	24		
N_r	2000	250	250	800		

a chance is given to systems i and $i+1$ to exchange their configurations (note that at this moment system $i+1$ has undergone 8 Metropolis steps less than system i). The exchange is accepted with probability $P_{TMC} = 1$ if $\delta E = E_i - E_{i+1} < 0$ or $P_{TMC} = \exp(-\Delta\beta\delta E)$ otherwise. Here E_i is the numerical value of Hamiltonian (1) for system i and $\Delta\beta = 1/T_{i+1} - 1/T_i$; *(4)* 8 Metropolis steps are applied on system $i+1$ (regardless of the fact that the previous exchange have or have not been performed); *(5)* the above exchange is tried between systems $i+1$ and $i+2$; *(6)* the cycle ends after the 8 Monte Carlo steps for $i = n$, after which no configuration exchange is tried.

Since[18] in 3D $T_{SG} \sim x$ and the purpose of TMC is to overcome energy barriers that could be as high as T_{SG}, then we found necessary to choose the highest temperature $T_1 \gtrsim 2x$. It is also important to take ΔT small enough to allow frequent state exchanges between systems. This is fulfilled by taking $\Delta T \lesssim T/\sqrt{c_s N}$ where c_s is the specific heat per spin. We choose appropriate values for ΔT from inspection of plots (not shown) of the specific heat vs T in preliminary simulations of the smaller systems.[18]

Initially the n configurations were completely disordered. For details on how we chose equilibration times t_0 see Section II C. Time t_0 is particularly large outside the AF region, varying from at least 4×10^6 MC sweeps for $x = 0.7$ and a number of dipoles $N \geq 300$ up to 4×10^7 sweeps for $x = 0.2$ and $N = 200$. Instead, t_0 in the AF zone is as low as 8×10^5 for $x \geq 0.86$. Thermal averages were calculated over the time range $[t_0, 2t_0]$. We further averaged over N_r samples with different realizations of disorder. Each realization was run twice to permit the calculation of overlapping parameters (see Section II C). Values of the parameters for all TMC runs are given in Table I.

C. Measured quantities

Measurements were performed after two averagings: first over thermalized configurations and secondly over different realizations of the quenched disorder.

We begin by presenting the specific heat. It was extracted from the slope of the energy as a function of the temperature.

As for the staggered magnetization, also for a PAD model on the square lattice we find appropriate to define it as[5]

$$m = N^{-1} \sum_i (-1)^{x_i} \sigma_i \,, \tag{3}$$

where x_i is the X coordinate of site i. We calculated the probability distribution $P(m)$, as well as the moments $m_1 = \langle |m| \rangle$, $m_2 = \langle m^2 \rangle$, and $m_4 = \langle m^4 \rangle$, where $\langle \dots \rangle$ stands for the above–defined double averages. From these moments we calculated the kurtosis (known also as Binder's cumulant) of $P(m)$ as $g_m = (3 - m_4/m_2^2)/2$. All these quantities have proven to be good signatures for possible AF–paramagnetic phase transitions.

In order to look for SG behavior, we also calculated the Edwards–Anderson overlap parameter between two independent equilibrium configurations obtained from a pair of identical replicas evolving independently in time,[30]

$$q = N^{-1} \sum_j \phi_j \,, \tag{4}$$

where

$$\phi_j = \sigma_j^{(1)} \sigma_j^{(2)} \,, \tag{5}$$

$\sigma_j^{(1)}$ and $\sigma_j^{(2)}$ being the spins on site j of replicas labelled as (1) and (2). Clearly, q is a measure of the spin configuration overlap between the two replicas. As done for m, we also calculated the probability distribution $P(q)$ as well as the moments $q_1 = \langle |q| \rangle$, $q_2 = \langle q^2 \rangle$, and $q_4 = \langle q^4 \rangle$. The SG susceptibility χ_{SG} is given by $N q_2$. Finally, we also make use of the relative mean square deviation of q, $\Delta_q^2 = q_2/q_1^2 - 1$, and kurtosis $g = (3 - q_4/q_2^2)/2$.

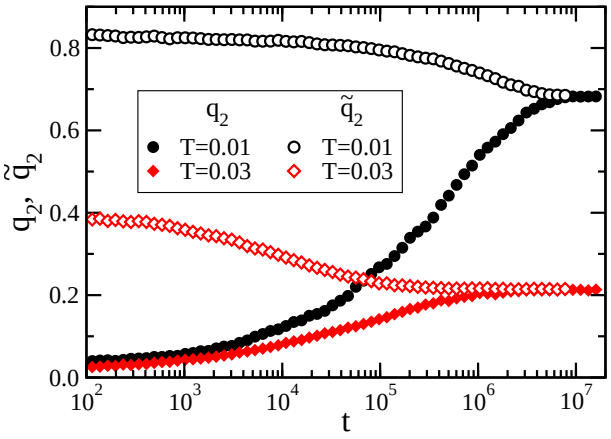

FIG. 1: (Color online) Semilog plots of $\widetilde{q}_2(t_0,t)$ and q_2 vs time t (in MC sweeps) for systems of 24×24 sites and concentration $x=0.5$ at the values of T shown in the legend. Here, q_2 comes from averages over time, starting from an initial random spin configuration at $t=0$. Here $t_0=8\times10^6$ MC sweeps. Data points at time t from an average over the time interval $[t,1.2t]$ and over 500 system samples.

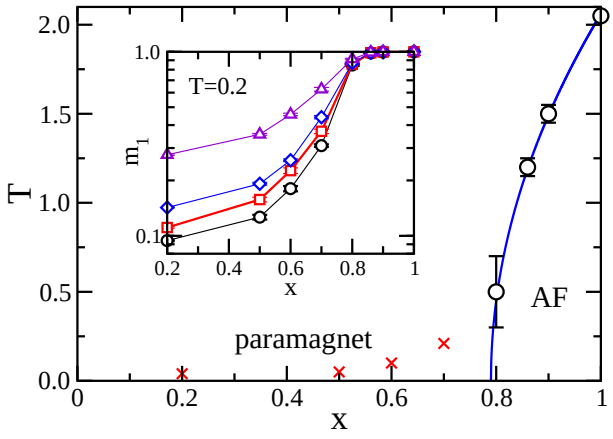

FIG. 2: (Color online) Phase diagram of the 2D PAD model. ∘ stand for the Néel temperature T_N and × for temperatures below which we cannot completely rule out a SG phase (see Section III). The full line for the phase boundary between the paramagnetic and AF phases is a fit to the data points given by $T_{AF}\simeq 4.5(x-x_c)^{1/2}$, where $x_c=0.79$. In the inset, m_1 versus x for $T=0.2$. ∘, □, ⋄, and △, stand for $L=24,20,16,$ and 8 respectively.

Let us explain now how t_0 was extracted. To make sure that equilibrium was reached, plots of q_2 and energy (average of H) were made over time intervals $[t,1.2t]$, not starting at $t=t_0$, as we do everywhere else, but starting at $t=0$, from an initial random spin configuration. Semilog plots of q_2 versus t displayed in Fig. 1 for $x=0.5$, $L=24$ and low temperatures show that a stationary state is reached only after some millions of MC sweeps. In order to check whether this state is truly in equilibrium, we define a time dependent spin overlap $\widetilde{q}$, not among pairs of identical systems, but among spin configurations of the same system at two different times t_0 and $t_1=t_0+t$ of the same TMC run,

$$\widetilde{q}(t_0,t)=N^{-1}\sum_j \sigma_j(t_0)\sigma_j(t_0+t). \qquad (6)$$

Let $\widetilde{q}_2(t_0,t)=\langle(\widetilde{q}(t_0,t))^2\rangle$. Suppose thermal equilibrium is reached at a time t'. Then, $\widetilde{q}_2(t_0,t)\to q_2$ as $t\to t'$ provided that $t_0\gtrsim t'$. Plots of $\widetilde{q}_2(t_0,t)$ vs t, for $10^{-5}t_0<t<t_0$ and $t_0=8\times10^6$ MC sweeps, are shown in Fig. 1. Note that both quantities, q_2 and $\widetilde{q}_2$ become approximately equal when $t\gtrsim10^6$ MC sweeps. In order to obtain equilibrium results, we have always chosen sufficiently large values of t_0 to make sure that, within errors, $\widetilde{q}_2(t_0,t)=q_2$ for $t\gtrsim t_0$. All values of t_0 are given in Table I.

In addition, we calculated a so–called correlation length for finite systems,

$$\xi_{x,L}=\frac{1}{2\sin(k/2)}\left[\frac{q_2}{\langle\mid q(\mathbf{k})\mid^2\rangle}-1\right]^{1/2}, \qquad (7)$$

where

$$k=\|\mathbf{k}\|, \qquad q(\mathbf{k})=N^{-1}\sum_j \phi_j e^{i\mathbf{k}\cdot\mathbf{r}_j}, \qquad (8)$$

$\mathbf{r}_j$ is the position of site j, and $\mathbf{k}=(2\pi/L,0)$. Recall that this system is anisotropic, as interactions along the spin axis are twice as large as in the perpendicular direction. Then, one could define a correlation length along the Y axis, $\xi_{y,L}$, by choosing $\mathbf{k}=(0,2\pi/L)$. We have found that $\xi_{x,L}$ is more convenient because it is less affected by finite–size effects than $\xi_{y,L}$. In order to compare with similar quantities defined for isotropic systems like the short–range 2D EA Ising model, we define also $\xi_L=(\xi_{x,L}+\xi_{y,L})/2$. In contrast to $P(q)$ and its first moments, ξ_L takes into account spatial variations of the EA overlap q and shows a good signature of SG transition. Its use has become customary in recent SG work.[22,31] Analogous expressions define the AF correlation length $\xi_L^{(m)}$ by substituting ϕ_j for $\psi_j=(-1)^{x_i}\sigma_i$ in Eqs.(7–8).

It is worth mentioning that in the $\xi_L/L\to0$ limit, ξ_L is, up to a multiplicative constant, the spatial correlation length of $\langle\phi_0\phi_r\rangle$. Therefore in the paramagnetic phase we can think of ξ_∞, the $L\to\infty$ limit of ξ_L, as the true correlation length of a macroscopic system. On the contrary, if there is strong long–range order with short–range order fluctuations (as predicted for the droplet model[24] for 3D SGs), $q_2\neq0$ (that is, $\langle\phi_0\phi_r\rangle$ does not vanish as $r\to\infty$) and $\langle\phi_0\phi_r\rangle-\langle\phi_0\rangle\langle\phi_r\rangle$ would be short–range. It then follows from its definition Eq.(7) that $\xi_L\sim L^2$ in 2D. Following current usage, we shall nevertheless refer to ξ_L as the "correlation length" .

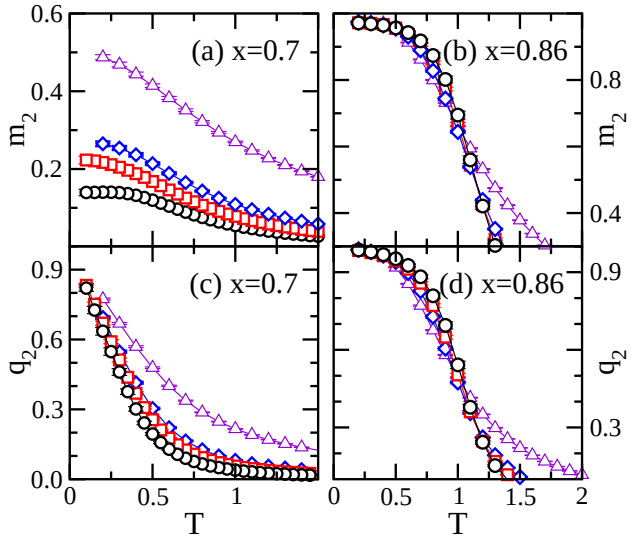

FIG. 3: (Color online) (a) Squared staggered magnetization m_2 vs T for $x = 0.7$. Icons ∘, □, ⋄, and △ stand for $L = 24, 20, 16$ and 8 respectively. Lines are only guides to the eye. Note that m_2 decreases with L at all temperatures consistently with absence of AF order. (b) Same as in (a) but for $x = 0.86$. Note that m_2 grows with L at low temperature, indicating an AF phase. (c) Same as in (a) but for the SG overlap parameter q_2. (d) Same as in (c) but for $x = 0.86$. Direct comparison of curves shown in panels (b) and (d) for $x = 0.86$ indicate a coupling between m_2 and q_2. This coupling does not occur for $x = 0.7$ (see panels (a) and (c)).

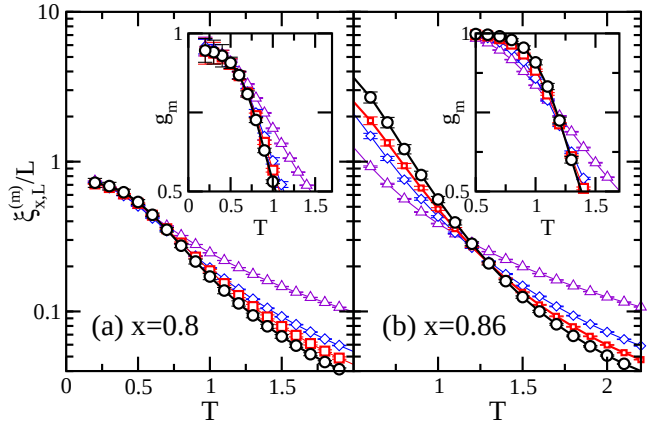

FIG. 4: (Color online) (a) Semilog plots of $\xi^{(m)}_{x,L}/L$ versus T for $x = 0.8$, and $L = 24$ (∘), $L = 20$ (□), $L = 16$ (⋄), and $L = 8$ (△). In the inset, kurtosis of the m distribution versus T for the same values of x and system sizes. (b) Same as in (a) but for $x = 0.86$.

III. RESULTS

A. The AF phase

The phase diagram shown in Fig. 2 summarizes our main results for the diluted 2D PAD model. For $x > x_c$ we find a thermally driven second order transition between the paramagnetic and AF phases at a Néel temperature $T_N(x)$ that vanishes as $x \to x_c$ from above. The phase boundary meets the $T = 0$ line at $x_c \simeq 0.79$. For concentrations well below x_c the paramagnetic phase covers the whole range $T \gtrsim 0$. We do not find evidence of a SG phase at finite temperature. However, our results are consistent with a SG correlation length that diverges algebraically near or at $T_{SG} = 0$. In the following we report the numerical evidence on which these qualitative results are based.

First we focus our attention on the paramagnetic–AF transition.[34] The AF phase is defined by the staggered magnetization (3). We illustrate in Fig. 3a how the moment of staggered magnetization m_2 behaves with temperature for $x = 0.7$. Note that m_2 appears to decrease as L increases even at low T. Plots of m_2 versus L (not shown) indicate a faster than algebraic decay in L, as one expects for a non AF phase. This is in sharp contrast to the behavior of m_2 for $x = 0.86$ (see Fig. 3b). Curves for different L cross at $T_N \simeq 1.15$. Below this temperature m_2 increases with L indicating the existence of an ordered AF phase. Similar results are obtained for higher values of x. In the inset of Fig. 2, plots of m_1 versus x for different system sizes at low temperature show that the system exhibits AF order for $x \gtrsim 0.8$. Similar graphs were obtained for m_2. These are our first pieces of evidence for the existence of an AF phase above $x_c \sim 0.8$. It is instructive to compare the behavior of m_2 with that of q_2 shown for $x = 0.86$ in Figs. 3b and 3d. m_2 and q_2 are not qualitatively different. This is not so for $x = 0.7$ where there is no AF order (compare Figs. 3a and 3c). From Fig. 3c it is not obvious whether q_2 vanishes or not as L increases at very low temperatures. We will return to this point in the discussion of Fig. 5.

For further information about the extent of the AF phase, we also examine how the cumulant–like quantity g_m and the finite–size AF correlation length behave for several pairs of values x, T. Let us first outline how g_m is expected to behave in the various magnetic phases. It clearly follows from its definition that $g_m \to 1$ as $L \to \infty$ in the case of long–range AF order. From the law of large numbers it also follows that $g_m \to 0$ as $L \to \infty$ in the paramagnetic phase. These two statements imply that curves of g_m vs T for various values of L cross at the phase boundary between the paramagnetic and AF phases. We make use of this fact to quantitatively determine the paramagnetic–AF phase boundary. Plots of g_m vs T are shown in the insets of Figs. 4a and 4b for $x = 0.8$ and 0.86, respectively. The signature of an AF phase below $T \simeq 1.2$ is clear for $x = 0.86$. The inset of Fig. 4a shows that within errors curves of g_m vs T for $x =$

0.8 and different system sizes merge instead of crossing at and below $T = 0.5(1)$. Note also that g_m does not go to 1 as $T \to 0$, indicating a broad distribution of $P(m)$ even in this limit. Finally, for $x < x_c$ (see Section III B), we find that g_m decreases as L increases for all T which is consistent with the absence of AF in this region.

In recent literature on SG phases the scale invariant finite–size correlation length[31] is frequently used to give evidence for a finite temperature transition, since ξ_L/L crosses at the transition temperature T_N and spreads out above and below T_N. The advantange of ξ_L/L over kurtosis is that the former may even diverge as $L \to \infty$ in contrast to the latter that tends to 1. Then we use the AF correlation length $\xi_L^{(m)}/L$ to pinpoint values for T_N by the value of T where curves cross. Recall that $\xi_L^{(m)}$ becomes a true correlation length when $\xi_L^{(m)}/L \ll 1$. Then, in the paramagnetic phase, $\xi_L^{(m)}/L \sim O(1/L)$, therefore decreasing as L increases. At T_N, $\xi_L^{(m)}/L$ must become size independent, as expected for a scale–free quantity. At lower temperatures, well in the long–range AF phase, we expect $\xi_L^{(m)}/L \sim O(L)$. Plots of $\xi_{x,L}^{(m)}/L$ versus T are shown in Figs. 4a and 4b for $x = 0.8$ and 0.86, respectively. Note that curves spread out above and below $T_N = 1.20(5)$ for $x = 0.86$. Similar graphs for $x = 0.9$ allow one to obtain the value $T_N = 1.50(5)$.

On the other hand curves merge for all temperatures below $T = 0.5(1)$ for $x = 0.8$ and $L \geq 16$ (see Fig. 4a), while m_2 decreases, within errors, algebraically with L for

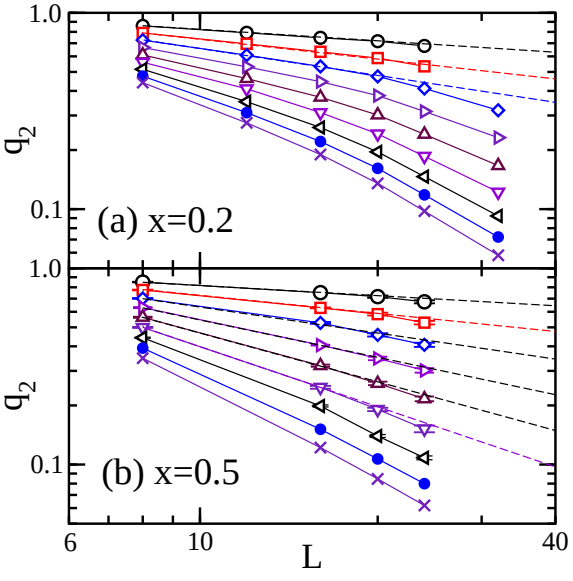

FIG. 5: (Color online) (a) Plots of q_2 versus L for $x = 0.2$. ○, □, ◇, ▷, △, ▽, ◁, ●, and × stand for $T/x = 0.2, 0.3, 0.4, 0.5, 0.6, 0.7, 0.8, 0.9,$ and 1.0 respectively. Lines are to guide the eye. Clearly, data for $T/x \gtrsim 0.4$ deviate from the straight dashed lines implying faster than a power of $1/L$ decay. (b) Same as in (a) but for $x = 0.5$. Here, only data for $T/x \gtrsim 0.7$ decay faster than a power of $1/L$. For all data, we have checked that, within errors, $\widetilde{q}_2 = q_2$.

the studied system sizes (not shown). It is interesting to note that graphs of the SG quantities g and ξ_L/L (instead of g_m and the AF $\xi_L^{(m)}/L$) give qualitatively the same picture when plotted versus T except from the fact that $g \to 1$ as $T \to 0$ for all x. Thus, the most straightforward interpretation of the data shown in Fig. 4a is that for all temperatures below $T = 0.5$ the system is near or at the AF phase boundary and its behavior displays criticality.

We have thus established all points of the AF phase boundary shown in Fig. 2 for $x > 0.7$. A fit to these data points, given by $T_N \simeq 4.5(x - x_c)^{1/2}$, where $x_c = 0.79(5)$ is shown in Fig. 2. Finally, for $x \leq 0.7$ (see below) we find that $\xi_L^{(m)}/L$ decreases as L increases for all T, as expected.

B. Very diluted systems

This Section is devoted to show the numerical results drawn for distributions of q and their first moments, and for ξ_L for systems with weak concentration. As for 3D PADs,[18] we expect universal behavior for $x \ll 1$ which enables us to compare our results with previous work. Thus, we direct our attention on the results we have obtained for $x = 0.2$ and $x = 0.5$. Both values are well

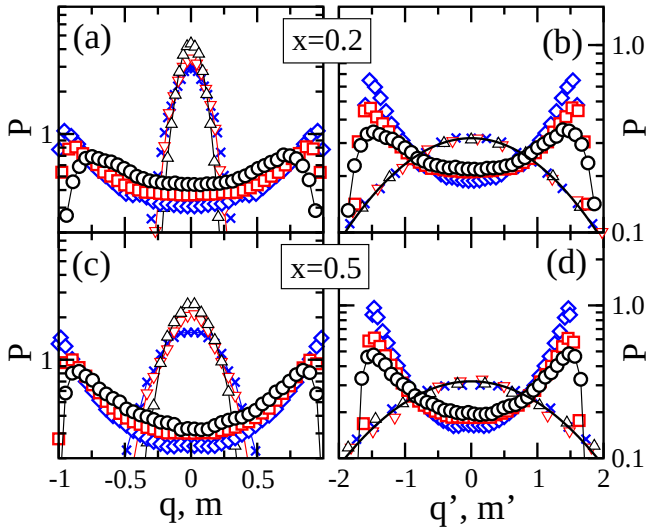

FIG. 6: (Color online) (a) Plots of the probability distributions $P(q)$ versus q, and $P(m)$ versus m both for $x = 0.2$ and $T/x = 0.4$. ○, □, ◇ are for $P(q)$ and system sizes $L = 32, 24$ and 20, respectively. △, ▽, and × are for $P(m)$ and system sizes $L = 24, 20$ and 16, respectively. (b) Same as in (a) but for the scaled distributions $P(q')$ versus $q' = q/q_1$, and $P(m')$ versus $m' = m/m_1$. The thick dashed line corresponds to the Gaussian distribution of paramagnets in the macroscopic limit. (c) Same as in (a) but for $x = 0.5$ and $T/x = 0.4$. ○, □, ◇ are for $P(q)$ and system sizes $L = 24, 20$ and 16, respectively. △, ▽, and × are for $P(q)$ and system sizes $L = 24, 20$ and 16, respectively. (d) Same as in (b) but for $x = 0.5$ and $T/x = 0.4$.

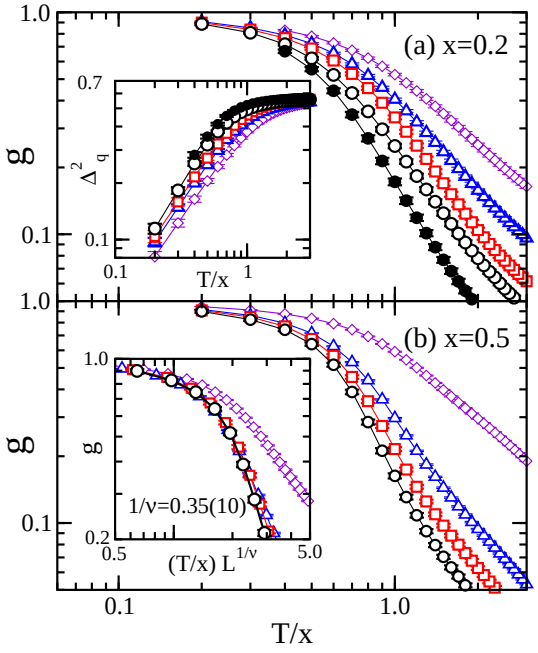

FIG. 7: (Color online) Kurtosis g of the distribution of q versus T/x for $x = 0.2$. •, ○, □, △, and ◇ stand for system sizes $L = 32, 24, 20, 16,$ and 8 respectively. In the inset, semilog plot of the relative mean square deviation Δ^2_q versus T/x for the same x and system sizes. Lines are guides to the eye. (b) Same as in (a) but for $x = 0.5$. ○, □, △, and ◇, stand for $L = 24, 20, 16,$ and 8 respectively. In the inset, scaling plot (g as a function of $(T/x)L^{1/\nu}$) of the data shown in the main figure.

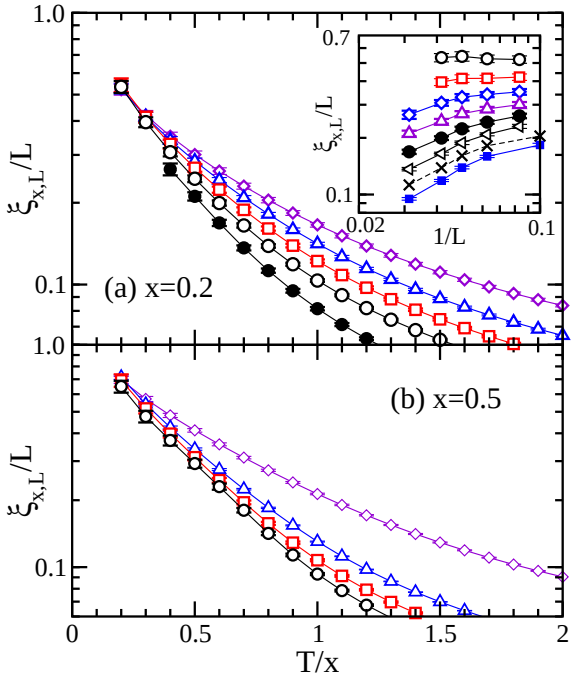

FIG. 8: (Color online) (a) Semilog plots of (a) SG correlation length divided by system size $\xi_{x,L}/L$ versus T/x for $x = 0.2$, and $L = 32$ (•), $L = 24$ (○), $L = 20$ (□), $L = 16$ (△), $L = 12$ (◇), and $L = 8$ (×). Lines are guides to the eye. (b) Same as in (a) but for $x = 0.5$, and $L = 24$ (○), $L = 20$ (□), $L = 16$ (△), and $L = 8$ (◇). In the inset of Fig. (a), log–log plot of $\xi_{x,L}/L$ versus $1/L$ for $x = 0.2$. ○, □, ◇, △, •, ◁, ×, and ■ stand for $T/x = 0.2, 0.3, 0.4, 0.5, 0.6, 0.7, 0.8,$ and 1.0 respectively.

below the $x \geq x_c = 0.79$ region, in which AF appears at low temperatures.

A plot of q_2 versus T for $x = 0.7$ is shown in Fig. 3c. Qualitatively similar graphs are obtained for other values of x satisfying $x \lesssim x_c$. Note that q_2 decreases as L increases, even at low temperatures. It is difficult to deduce from these plots whether or not q_2 vanishes as $L \to \infty$ at low T. In order to elucidate this question we prepare log–log plots of q_2 vs L, shown in Figs. 5a and 5b for $x = 0.2$ and 0.5 respectively. Data points in these figures seem to be consistent with a decay faster than $q_2 \sim L^{-\eta}$ for $T/x \gtrsim 0.3$, indicating that we are in the paramagnetic phase. Plots of q_1 vs L show the same qualitative behavior. Altogether these results leave small room for the existence of a SG phase with quasi–long range order at very low temperatures, as it has been reported for the 3D diluted PAD model for $T/x \gtrsim 1$.

Next we report results for the distributions of m and q at low temperature. Due to the central limit theorem and since the correlation lengths are finite in the paramagnetic phase, $P(m)$ and $P(q)$ are expected to be normal distributions for $L = \infty$. The droplet picture[24] for SG's predicts that $P(q) = [\delta(q + q_0) + \delta(q - q_0)]/2$ where q_0 is the EA order parameter, and that the tail of $P(q)$ down to $q = 0$ for finite–size systems vanishes as L increases. On the contrary, the RSB picture[23] predicts a nontrivial distribution with a non–vanishing $P(q = 0)$ which is size independent. Plots of $P(q)$ and $P(m)$ are shown for $x = 0.2$ and $x = 0.5$ for $T/x = 0.4$ in Figs. 6a–6c. All distributions depend on L. $P(m)$ are found to be normally distributed. In Figs. 6b and 6d normalized distributions of the reduced quantity $m' = m/m_1$ are shown. Note that $P(m') \simeq (1/\pi)\exp(-m'^2/\pi)$ for the studied system sizes, indicating complete absence of AF order. On the other hand, $P(q)$ are found to be double peaked distributions. As L increases, their peak positions shift towards $q = 0$ and $P(0)$ increases. Neither the droplet nor the RSB models consent a fit to these data. If it turns out that our systems are near or at criticality, then $P(q')$ (where $q' = q/q_1$) ought to be size independent. However, reduced distributions $P(q')$ in Figs. 6b–6d are shown to have an L dependence. We conclude that our results are only consistent with a paramagnetic phase. Similar conclusions apply for $T/x \gtrsim 0.2$.

In the same way as explained in Section III A for quantities g_m and $\xi^{(m)}_L/L$, their dimensionless SG counterparts g and ξ_L/L, as well as Δ^2_q, indicate the location of the temperature T_{SG} of a SG transition. Recall that, according to the finite–size scaling assumption, all these quantities depend only on $L(T - T_{SG})^\nu$ and then become size independent at T_{SG}. We are assuming that for large enough sizes, L/ξ (where ξ is the *true* correlation length)

is the only relevant parameter and $\xi \sim (T - T_{SG})^{-\nu}$. Plots of g vs T/x are given in Fig. 7a and 7b for $x = 0.2$ and 0.5 respectively. It seems that curves of g for various values of L do not cross and only merge as $T \to 0$. This is consistent with $T_{SG} = 0$ in accordance with the behavior of 2D EA systems, although a merging at $T/x \approx 0.2$ is not completely excluded within errors. We found more useful to study Δ_q^2, which has a direct interpretation as the uncertainty of q/q_1 and could be computed with higher precision as it involves lower moments of[14] $P(q)$. A plot of Δ_q^2 vs T/x for $x = 0.2$ is shown in the inset of Fig. 7a. Clearly, Δ_q^2 increases with L for all $T/x \geq 0.2$ as expected for a paramagnetic phase and contrary to the expected behavior $\Delta_q^2 \to 0$ for increasing L in a SG phase with non–vanishing order parameter. A similar behavior for $x = 0.5$ is observed (not shown).

We now turn our interest to the behavior of the SG finite–size correlation length ξ_L/L. Similarly to g, ξ_L/L is independent of L at T_{SG} as it corresponds to be for a scale–free quantity. On the other hand, well inside the paramagnetic phase, ξ_L/L should diminish as $O(1/L)$, provided $\xi_L/L \ll 1$. Figs. 8a and 8b show data for $\xi_{x,L}$ as a function of T/x for several system sizes, for $x = 0.2$ and 0.5 respectively. Curves do not cross at any finite temperature and $\xi_{x,L}/L$ decrease as L increases at least for $T/x \gtrsim 0.4$. All curves seem to converge only as $T \to 0$ suggesting $T_{SG} = 0$. Plots for $\xi_{x,L}$ vs L (see inset of Fig. 8a) are consistent with an algebraic decay $\xi_{x,L}/L \sim L^{-y}$ for temperatures $T/x \gtrsim 0.4$ and system sizes $L \geq 16$. For lower temperatures, data do not vary very much as L increases and so we cannot definitely rule out a non–vanishing $\xi_{x,L}/L$ in the thermodynamic limit. Consequently, from Fig. 8 alone, a transition at very low, but not zero, temperature cannot be completely excluded.

C. The ν exponent at $T_{SG} = 0$

Our results concur with the behavior found for a random–bond 2D RAD model with dipolar interactions,[14] and the one found time ago for 2D EA models.[25] Recent simulations for the latter (with larger system sizes and lower T) including nearest–neighbor exchange interactions find a lower value $1/\nu = 0.29(4)$ for Gaussian distributions,[26] but do not provide conclusive results for bimodally distributed interactions.[28] A scenario has been proposed where these models for varying realizations of disorder belong to the same universality class at non–zero temperatures,[27] even though their respective behaviors differ at $T = 0$.

Let us assume that $T_{SG} = 0$ and that ξ diverges as $\xi \sim T^{-\nu}$. According to finite–size scaling, dimensionless quantities like g and ξ_L/L should scale as

$$g = G(TL^{1/\nu}), \quad \xi_L/L = X(TL^{1/\nu}). \tag{9}$$

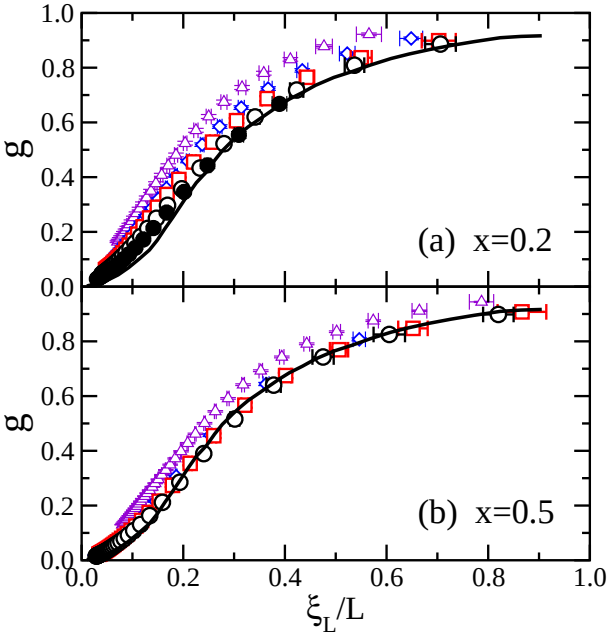

FIG. 9: (Color online) (a) Kurtosis g as a function of the finite–size correlation length divided by system size, ξ_L/L for $x = 0.2$. •, ○, □, ◇, and △ stand for $L = 32, 24, 20, 16$, and 12 respectively. All data should collapse onto an universal curve, provided that scaling corrections are small. The thick continuous line stands for the universal curve that corresponds to the 2D Ising SG model with short–range interactions. (b) Same as in (a) but for $x = 0.5$. ○, □, ◇, and △ stand for system sizes $L = 24, 20, 16$, and 8 respectively.

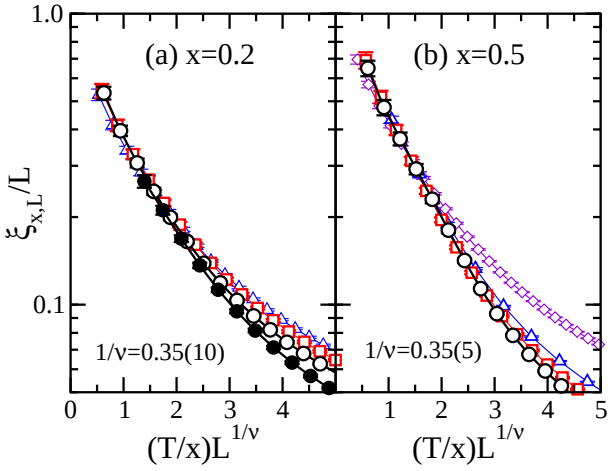

FIG. 10: (Color online) (a) Scaling plot for the SG correlation length divided by system size, $\xi_{x,L}/L$ versus $(T/x)L^{1/\nu}$ with $1/\nu = 0.35$ for $x = 0.2$. •, ○, □, and △ are for $L = 32, 24, 20$ and 16, respectively. (b) Same as in (a) but for $x = 0.5$. ○, □, △, and ◇ are for $L = 24, 20, 16$ and 8, respectively. Error bars, where not shown, are smaller than symbols.

It follows that $g = F(\xi_L/L)$, where F is in principle a non–universal function that, apart from the bulk universality class, depends on the boundary conditions (we

chose them to be periodic), the sample shapes (squared lattices), as well as the anisotropy[35] of the interactions. Plots of g versus ξ_L/L are shown in Figs. 9a and 9b for $x = 0.2$ and 0.5 respectively. Data for different values of L and x should collapse into a single scaling curve, on condition that finite–size effects are small. This is what we find for systems with $N \gtrsim 100$. However, for smaller N curves spread out indicating that finite–size scaling corrections are large. It is remarkable that data seems to collapse onto the universal scaling curve found for the (isotropic) 2D EA models mentioned above in this Section,[26,28] specially at low T. Note that in Figs. 9a and 9b we use ξ_L/L instead of $\xi_{x,L}/L$ in order to average anisotropic effects over the two principal axes of the underlying square lattice. This suggests that both, 2D PAD and short–range EA models, may share a common universality class. However, large correlations to scaling for the available system sizes prevent us to go further on this direction.

Scaling plots of $\xi_{x,L}/L$ versus $(T/x)L^{1/\nu}$ are shown in Figs. 10a and 10b for $x = 0.2$ and $x = 0.5$ respectively. Due to the presence of large finite–size corrections, no value of $1/\nu$ allows to collapse all data in one single curve. We have chosen $1/\nu$ in order to allow data collapse for large L and low T. We find that $1/\nu = 0.35$ is a suitable value in both cases. Scaling plots become significantly worse (not shown) when using values of $1/\nu$ outside the interval $[0.25, 0.45]$ ($[0.3, 0.4]$) for $x = 0.2$ ($x = 0.5$). That gives a rough estimate of the error on $1/\nu$. A scaling plot of g versus $(T/x)L^{1/\nu}$ is shown in the inset of Fig. 7b for $x = 0.5$. Again, $1/\nu = 0.35(10)$ allows to scale data for large L and low T, which is consistent with the value extracted from $\xi_{x,L}/L$. The value $1/\nu = 0.35(10)$ also agrees with the effective exponent found in old simulations of the 2D EA model for small system sizes and relatively high temperatures and is slightly larger than the value $1/\nu = 0.29(4)$ found in recent simulations for the same models (but the two values are still consistent within errors). In any case, such discrepancies may be caused by the fact that finite–size scaling corrections are important for the limited system sizes that we were able to simulate.

IV. CONCLUSIONS

By tempered Monte Carlo calculations, we have studied a diluted dipolar Ising model on a square lattice. There are only dipole–dipole interactions. Spins randomly occupy only a fraction x of all lattice sites. The entire phase diagram of the system, in particular the boundary between the AF and the paramagnetic phases, has been explored and it is shown in Fig. 2. We have also provided strong evidence that the paramagnetic phase covers the whole $T > 0$ range for $x < x_c$, where $x_c = 0.79(5)$. From the behavior of the spin–glass (SG) overlap q, the relative mean square deviation Δ_q^2, kurtosis g, and ξ_L/L, we conclude that $T_{SG} = 0$ for $x < x_c$, and there is an algebraic divergence of the correlation length with an exponent $1/\nu = 0.35(10)$. All these properties are consistent with the behavior found for the 2D diluted RAD and 2D EA model with short–range interactions. This is to be contrasted with the manifestly different behavior found for the 3D PAD (quasi long–range order at low T) and the 3D EA model (with a non–vanishing order parameter in the SG phase).

Acknowledgments

We thank Julio F. Fernández for helpful discussions and reading the manuscript. We are indebted to the Centro de Supercomputación y Bioinformática and to the Applied Mathematics Department both at University of Málaga (Spain), to Institute Carlos I at University of Granada (Spain) and to the SP6 computer array at CINECA in Bolonia (Italy) for much computer time. JJA thanks financial support from a Junta de Andalucía Grant FQM–278–2010.

* E-mail address: jjalonso@uma.es
† E-mail address: alles@df.unipi.it

[1] R. P. Cowburn, Philos. Trans. R. Soc. London, Ser. A **358**, 281 (2000); R. J. Hicken, *ibid.* **361**, 2827 (2003).
[2] R. F. Wang, C. Nisoli, R. S. Freitas, J. Li, W. McConville, B. J. Cooley, M. S. Lund, N. Samarth, C. Leighton, V. H. Crespi and P. Schiffer, Nature (London) **439**, 303 (2006); G. A. Held, G. Grinstein, H. Doyle, S. Sun and C. B. Murray, Phys. Rev. B **64**, 012408 (2001).
[3] S. A. Majetich and M. Sachan, J. Phys. D: Appl. Phys. **39**, R407 (2006).
[4] J. Luttinger and L. Tisza, Phys. Rev. **70**, 954 (1946); J. Luttinger and L. Tisza, *ibid.* **72**, 257 (1947).
[5] J. F. Fernández and J. J. Alonso, Phys. Rev. B **62**, 53 (2000).
[6] K. Yamamoto, S. A. Majetich, M. R. McCartney, M. Sachan, S. Yamamuro and T. Hirayama, Appl. Phys. Lett. **93**, 082502 (2008); M. Georgescu, J. L. Viota, M. Klokkenburg, B. H. Erné, D. Vanmaekelbergh and P. A. Zeijlmans van Emmichoven, Phys. Rev B **77**, 024423 (2008).
[7] Y. Takagaki, C. Herrmann and E. Wiebicke, J. Phys.: Condens. Matter **20**, 225007 (2008).
[8] K. De'Bell, A. B. McIsaac, I. N. Booth and J. P. Whitehead, Phys. Rev. B **55**, 15108 (1997); J. J. Alonso and J. F. Fernández, Phys. Rev. B **74**, 184416 (2006).
[9] S. J. Knak Jensen and K. Kjaer, J. Phys.: Condens. Matter **1**, 2361 (1989).
[10] W. Luo, S. R. Nagel, T. F. Rosenbaum and R. E. Rosensweig, Phys. Rev. Lett. **67**, 2721 (1991).
[11] D. Gateschi and R. Sessoli, *Magnetism: Molecules to materials*, edited by J.S. Miller and M. Drillon (Wiley–VCH, Weinheim, 2002), Vol. III, Chap.3.

[12] D. H. Reich, B. Ellman, J. Yang, T. F. Rosenbaum, G. Aeppli and D. P. Belanger, Phys. Rev. B **42**, 4631 (1990); J. A. Griffin, M. Huster and R. J. Folweiler, Phys. Rev. B **22**, 4370 (1980).

[13] T. Jonsson, J. Mattsson, C. Djurberg, F. A. Khan, P. Nordblad and P. Svedlindh, Phys. Rev. Lett. **75**, 4138 (1995); F. Bert, V. Dupuis, E. Vincent, J. Hammann and J.–P. Bouchaud, Phys. Rev. Lett. **92**, 167203 (2004); G. G. Kenning, G. F. Rodriguez and R. Orbach, Phys. Rev. Lett. **97**, 057201 (2006).

[14] J. F. Fernández, Phys. Rev. B **78**, 064404 (2008); J. F. Fernández and J. J. Alonso, Phys. Rev. B **79**, 214424 (2009).

[15] K.–M. Tam and M. J. P. Gingras, Phys. Rev. Lett. **103**, 087202 (2009).

[16] W. Wu, D. Bitko, T. F. Rosenbaum and G. Aeppli, Phys. Rev. Lett. **71**, 1919 (1993); J.A. Quilliam, S. Meng, C. G. A. Mugford and J. B. Kycia, Phys. Rev. Lett., **101** 187204 (2008); C. Ancona–Torres, D. M. Silevitch, G. Aeppli and T. F. Rosenbaum, Phys. Rev. Lett. **101** 057201 (2008);

[17] P. E. Jönsson, R. Mathieu, W. Wernsdorfer, A. M. Tkachuk and B. Barbara, Phys. Rev. Lett. **98**, 256403 (2007)

[18] J. J. Alonso and J. F. Fernández, Phys. Rev. B **81**, 064408 (2010).

[19] J. M. Kosterlitz and D. J. Thouless, J. Phys. C **6**, 1181 (1973); J. M. Kosterlitz, *ibid.* **7**, 1046 (1974); see also J. V. José, L. P. Kadanoff, S. Kirkpatrick and D. R. Nelson, Phys. Rev. B **16**, 1217 (1977); J. Villain, J. Phys. (Paris) **36**, 581 (1975). J. F. Fernández, M. F. Ferreira and J. Stankiewicz, Phys. Rev. B **34**, 292 (1986); H. G. Evertz and D. P. Landau, Phys. Rev. B **54**, 12302 (1996).

[20] A. J. Bray, M. A. Moore and A. P. Young, Phys. Rev. Lett. **56**, 2641 (1986).

[21] H. G. Katzgraber and A. P. Young, Phys. Rev. B **67**, 134410 (2003); H. G. Katzgraber and A. P. Young, Phys. Rev. B **72**, 184416 (2005); H. G. Katzgraber, D. Larson and A. P. Young, Phys. Rev. Lett. **102**, 177205 (2009).

[22] H. G. Katzgraber, M. Körner and A. P. Young, Phys. Rev. B **73**, 224432 (2206); M. Hasenbusch, A. Pelissetto and E. Vicari, Phys. Rev. B **78**, 214205 (2008).

[23] G. Parisi, Phys. Rev. Lett. **43**, 1754 (1979); *ibid* **50**, 1946 (1983); for reviews, see M. Mézard, G. Parisi and M. A. Virasoro, *Spin Glass Theory and Beyond* (World Scientific, Singapore, 1987); E. Marinari, G. Parisi and J. J. Ruiz–Lorenzo, in *Spin Glasses*, edited by K. H. Fischer and J. A. Hertz, (Cambridge University Press, Cambridge, 1991); E. Marinari, G. Parisi, F. Ricci–Tersenghi, J. J. Ruiz–Lorenzo and F. Zuliani, J. Stat. Phys **98**, 973 (2000).

[24] D. S. Fisher and D. A. Huse, J. Phys. A **20**, L1005 (1987); D. A. Huse and D. S. Fisher, *ibid.* **20**, L997 (1987); D. S. Fisher and D. A. Huse, Phys. Rev. B **38**, 386 (1988).

[25] M. Ney–Nifle and A. P. Young, J. Phys. A **30**, 5311 (1997); S. Liang, Phys. Rev. Lett. **69**, 2145 (1992). A value $1/\nu = 0.38(6)$ was reported in R. N. Bhatt and A. P. Young, Phys. Rev. B **37**, 5606 (1988);

[26] H. G. Katzgraber, L. W. Lee and A. P. Young, Phys. Rev. B **70**, 014417 (2004); J. Houdayer and A. K. Hartmann, Phys. Rev. B **70**, 014418 (2004).

[27] T. Jörg, J. Lukic, E. Marinari and O. C. Martin, Phys. Rev. Lett. **96**, 237205 (2006);

[28] H. G. Katzgraber, L. W. Lee and I. A. Campbell, Phys. Rev. B **75**, 014412 (2007).

[29] E. Marinari and G. Parisi, Europhys. Lett. **19**, 451 (1992); K. Hukushima and K. Nemoto, J. Phys. Soc. Jpn. **65**, 1604 (1996).

[30] S. F. Edwards and P. W. Anderson, J. Phys. F, **5**, 965 (1975).

[31] M. Palassini and S. Caracciolo, Phys. Rev. Lett. **82**, 5128 (1999); H. G. Ballesteros, A. Cruz, L. A. Fernández, V. Martín–Mayor, J. Pech, J. J. Ruiz–Lorenzo, A. Tarancón, P. Téllez, C. L. Ullod and C. Ungil, Phys. Rev. B **62**, 14237 (2000).

[32] P. Ewald, Ann. Phys. **369**, 253 (1921).

[33] N. A. Metropolis, A. W. Rosenbluth, M. N. Rosenbluth, A. H. Teller and E. Teller, J. Chem. Phys. **21**, 1087 (1953).

[34] For a study of the paramagnetic–AF phase transition, as well as properties of the AF phase on fully occupied SC lattices, see Ref.[5] and J. F. Fernández, Phys. Rev. B **66**, 064423 (2002).

[35] W. Selke and L. N. Shchur, J. Phys. A: Math. Gen. **38**, L739 (2005).